Endosomal maturation by Rab conversion in *Aspergillus nidulans* is coupled to dynein-mediated basipetal movement

Juan F. Abenza*, Antonio Galindo, Mario Pinar, Areti Pantazopoulou, Vivian de los Ríos, and Miguel A. Peñalva

Departamento de Medicina Molecular y Celular, Centro de Investigaciones Biológicas del Consejo Superior de Investigaciones Cientificas, 28040 Madrid, Spain

ABSTRACT **We exploit the ease with which highly motile early endosomes are distinguished from static late endosomes in order to study *Aspergillus nidulans* endosomal traffic. RabS^{Rab7} mediates homotypic fusion of late endosomes/vacuoles in a homotypic fusion- and vacuole protein sorting/Vps41–dependent manner. Progression across the endocytic pathway involves endosomal maturation because the end products of the pathway in the absence of RabS^{Rab7} are minivacuoles that are competent in multivesicular body sorting and cargo degradation but retain early endosomal features, such as the ability to undergo long-distance movement and propensity to accumulate in the tip region if dynein function is impaired. Without RabS^{Rab7}, early endosomal Rab5s—RabA and RabB—reach minivacuoles, in agreement with the view that Rab7 homologues facilitate the release of Rab5 homologues from endosomes. RabS^{Rab7} is recruited to membranes already at the stage of late endosomes still lacking vacuolar morphology, but the transition between early and late endosomes is sharp, as only in a minor proportion of examples are RabA/RabB and RabS^{Rab7} detectable in the same—frequently the less motile—structures. This early-to-late endosome/vacuole transition is coupled to dynein-dependent movement away from the tip, resembling the periphery-to-center traffic of endosomes accompanying mammalian cell endosomal maturation. Genetic studies establish that endosomal maturation is essential, whereas homotypic vacuolar fusion is not.**

Monitoring Editor
Patrick J. Brennwald
University of North Carolina

Received: Nov 16, 2011
Revised: Mar 1, 2012
Accepted: Mar 20, 2012

INTRODUCTION

The mechanisms by which membrane and associated proteins traffic across the endocytic pathway toward degradative organelles (metazoan lysosomes and fungal vacuoles) have been intensively investigated (Huotari and Helenius, 2011). Rather than being vesicle mediated, traffic between early endosomes (EEs) and late endosomes (LEs) occurs by maturation. According to this view, EEs, which receive biosynthetic traffic from the Golgi, progressively undergo changes in lumenal pH and composition as they fuse homotypically to give rise to gradually larger organelles. Simultaneously, portions of endosomal membranes that are sorted into the multivesicular body pathway bud inward, thereby delivering lipids and their associated proteins into the lumen of the organelle. Thus maturation results in organelles that are larger than EEs and display a characteristic multivesicular appearance. These multivesicular, "late" endosomes undergo further fusion between themselves and with the vacuoles/lysosomes, thus making their cargo accessible to digestion by the vacuolar/lysosomal hydrolases.

Rabs are small GTPases that, when switched to their GTP conformation, associate with intracellular membranes, recruiting to them "effector" interacting proteins from the cytosol (Behnia and Munro, 2005). These effectors include tethers, soluble *N*-ethylmaleimide–sensitive factor attachment protein receptor (SNARE) regulators, and lipid-modifying enzymes that are major determinants of membrane identity (Zerial and McBride, 2001; Pfeffer and Aivazian, 2004).

This article was published online ahead of print in MBoC in Press (http://www.molbiolcell.org/cgi/doi/10.1091/mbc.E11-11-0925) on March 28, 2012.

*Present address: The Wellcome Trust/Cancer Research UK Gurdon Institute, University of Cambridge, Cambridge CB2 1QN, United Kingdom.

Address correspondence to: Miguel A. Peñalva (penalva@cib.csic.es).

Abbreviations used: CMAC, 7-amino-4-chloromethyl-coumarin; CORVET, class C core vacuole/endosome tethering; EE, early endosome; GDI, GDP dissociation inhibitor; GEF, guanine nucleotide exchange factor; GST, glutathione *S*-transferase; HOPS, homotypic fusion and vacuole protein sorting; MT, microtubule.

Owing to the high specificity of any given Rab for a certain membrane, Rabs have been extensively used in membrane traffic studies, including endosomal maturation itself, as the transition between EEs and LEs appears to be mediated by Rab conversion (Rink *et al.*, 2005; Segev, 2011). In its simplest version, Rab conversion implies that early endosomal membrane domains containing Rab5 are converted into late endosomal domains containing Rab7. As a result, Rab7 effectors substitute for Rab5 effectors, leading to a shift in compartmental identity toward LEs. Replacement of Rab5 by Rab7 on endosomes requires that the positive feedback loops that stabilize Rab5 domains (Zerial and McBride, 2001) need to be inactivated, and the mechanisms facilitating Rab7 recruitment need to be activated coordinately (Rink *et al.*, 2005; Nordmann *et al.*, 2010; Segev, 2011).

Major insight into the mechanisms of endosomal maturation came from work with *Saccharomyces cerevisiae* (Price *et al.*, 2000; Peplowska *et al.*, 2007; Markgraf *et al.*, 2009; Brocker *et al.*, 2010; Cabrera *et al.*, 2010; Nordmann *et al.*, 2010; Ostrowicz *et al.*, 2010). Endosomal Rab conversion results in substitution of the Vps21p (i.e., Rab5) effector class C core vacuole/endosome tethering (CORVET) complex (Peplowska *et al.*, 2007) by the Ypt7p (i.e., Rab7) effector homotypic fusion and vacuole protein sorting (HOPS) complex (Seals *et al.*, 2000). However, the actual mechanism by which HOPS substitutes for CORVET has not been established. Both HOPS and CORVET are multiprotein complexes that share four class C proteins—Vps11p, Vps16p, Vps18p, and Vps33p (Rieder and Emr, 1997)—and only differ in two specific components each—Vps8p and Vps3p for CORVET and Vps41 and Vps39 for HOPS.

A hurdle hindering correlation between subcellular and mechanistic studies of endosomes is implicit in the maturation concept: by definition, the distinction between EEs and LEs is unavoidably blurred (Huotari and Helenius, 2011). The basidiomycete *Ustilago maydis* and the ascomycete *Aspergillus nidulans* are ideally suited for studying endosomal maturation because their EEs can be unequivocally identified by their characteristic long-distance bidirectional movement on microtubule-dependent motors (Wedlich-Soldner *et al.*, 2002; Lenz *et al.*, 2006; Steinberg, 2007; Zekert and Fischer, 2008; Abenza *et al.*, 2009, 2010; Hervás-Aguilar *et al.*, 2010; Peñalva, 2010; Zhang *et al.*, 2010, 2011; Schuster *et al.*, 2011).

A. nidulans has two Rab5 paralogues—RabA and RabB—localizing to EEs (Abenza *et al.*, 2009, 2010) and a single Rab7 homologue (Ohsumi *et al.*, 2002; Sánchez-Ferrero and Peñalva, 2006), which we denoted RabS (Rab seven, RabS^{Rab7}). The CORVET complex is an effector of RabB and, to a lesser extent, of RabA (Abenza *et al.*, 2010). Whether HOPS is a RabS^{Rab7} effector was unknown. Because maturation involves the CORVET-mediated coalescence of EEs into progressively larger endosomes (Markgraf *et al.*, 2009), it seems plausible that the resulting increase in size inevitably results in decreased motility. Such decreased motility would be a bona fide feature of LEs. Indeed, overexpression of the CORVET recruiters RabA/RabB leads to formation of endosomal aggregates with reduced motility and multivesicular appearance (a landmark of LEs; Abenza *et al.*, 2009, 2010; Griffith *et al.*, 2011). However, as discussed by Huotari and Helenius (2011), the presence of internal vesicles cannot be the sole criterion to define LEs. Indeed ESCRT-III appears to operate in *A. nidulans* EEs (Galindo *et al.*, 2007; Hervás-Aguilar *et al.*, 2010). LEs and vacuoles can be visualized with 7-amino-4-chloromethyl-coumarin (CMAC), a fluorescent compound that labels the lumen of hydrolase-containing acidic organelles, including vacuoles and smaller structures. Here we use the term "vacuole" to refer to spherical CMAC-positive organelles whose limiting membrane is stainable with FM4-64 (Peñalva, 2005). However, the limiting membrane/shape of the smaller CMAC-positive structures cannot be resolved by optical microscopy. Thus we will use the generic term "LE/vacuole" to collectively refer to all "mature" structures that are CMAC positive, irrespective of their size.

Here we characterize in detail RabS^{Rab7} and demonstrate that it localizes to vacuoles and to smaller structures, that HOPS is a RabS^{Rab7} effector, and that deletion of *rabS* leads to the formation of small yet proteolytically competent CMAC-positive structures that, unlike normal vacuoles, undergo long-distance movement and contain early endosomal Rabs in their membranes. Time-lapse analyses showed that the transition between RabA/B-containing EEs and RabS^{Rab7} structures is sharp, although colocalization can be detected on large (and thus less motile) endosomal aggregates. Dynein impairment results in the accumulation of vacuoles in a region near the tip that is normally devoid of them. Taken together, our data support a model in which endosomal maturation progresses as endosomes move away from the tip, losing motility as they enlarge through homotypic fusion.

RESULTS

RabS^{Rab7} localizes to the vacuolar membranes

We studied the localization of green fluorescent protein (GFP)–tagged or mCherry-tagged versions of RabS^{Rab7} with constructs containing the *rabS* promoter or the regulatable promoter *alcA*^{p}. All constructs were single-copy integrated into the genome by targeted recombination (Calcagno-Pizarelli *et al.*, 2007). Anti-GFP Western analysis, used to determine the levels of GFP-RabS^{Rab7} expression obtained with the *alcA*^{p} driver, showed that these were below detection on glucose (*alcA*^{p}-repressing conditions), very high on ethanol (*alcA*^{p}-inducing conditions), and low on 0.1% fructose (noninduced, nonrepressed *alcA*^{p} conditions; Figure 1A). *alcA*^{p}-driven fructose levels were similar or slightly below those driven by the *rabS*^{p} (Figure 1B). Whether GFP or mCherry tagged, overexpressed (ethanol; Figure 1C) or expressed to approximately physiological levels (fructose; Figure 1D), RabS^{Rab7} robustly localizes to the membrane or spherical vacuoles whose lumen is stainable with the vacuolar tracer CMAC.

Rabs associate with membranes in their GTP conformation (Behnia and Munro, 2005). On GTP hydrolysis, GDP-Rabs are extracted to the cytosol by the GDP dissociation inhibitor (GDI; encoded by *A. nidulans gdiA*). Figure 1F shows that the vacuolar membrane localization of RabS^{Rab7} is strictly dependent on the nucleotide switch of the GTPase, as mutant Thr22Asn GFP-RabS^{Rab7}, locked in the GDP conformation, is cytosolic (Figure 1F), even though the mutation does not affect the steady-state protein levels (Figure 1E). This shows that GFP-RabS^{Rab7} reflects the physiological localization of RabS.

The size and relative abundance of vacuoles increase with the distance to the tip

We exploited the fact that RabS^{Rab7} specifically labels vacuoles to measure their distribution along hyphae. We determined the percentage of cell projection surface occupied by vacuoles in 30- to 60-μm-long germlings (n = 33), which were segmented into five zones (Figure 2A). Vacuoles occupied, on average, 40% of the conidiospore projection but only 9% of the region nearest to the tip. The regions between the tip and the base showed intermediate scores, the overall tendency being that vacuole-occupied surface increases with the distance to the tip. This increase correlates with a parallel increase in vacuolar diameter (Figure 1C; Peñalva, 2005; Findon *et al.*, 2010). Thus the biogenesis of vacuoles is connected to the relative position within hyphae, such that tip-proximal regions are

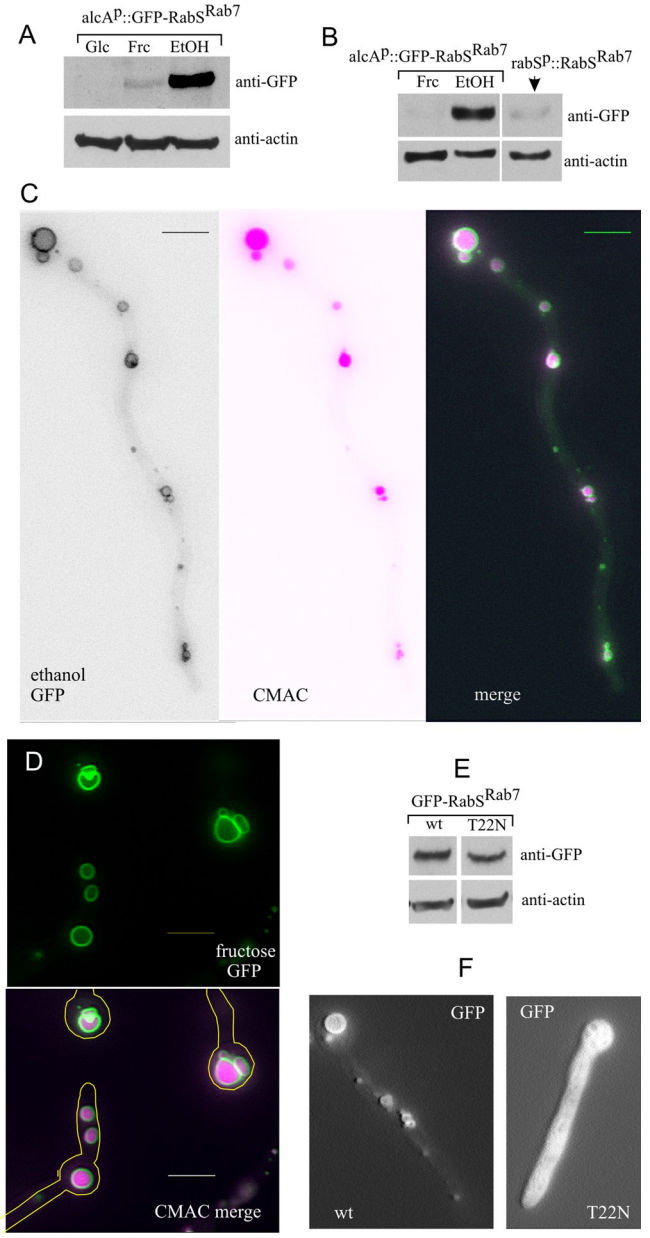

FIGURE 1: Subcellular localization of RabS^{Rab7}. (A) Anti-GFP Western blot analysis showing the different steady-state levels of GFP-RabS^{Rab7} achieved under repressing (1% glucose, Glc), noninducing, nonrepressing (0.1% fructose, Frc) and inducing (1% ethanol, EtOH) conditions for the *alcA*^{p} driver. Actin was used as loading control. (B) GFP-RabS^{Rab7} levels driven by the physiological promoter compared with those obtained with *alcA*^{p}. (C) Vacuolar localization of GFP-RabS^{Rab7} (*alcA*^{p} driver, ethanol conditions). (D) Vacuolar localization of GFP-RabS^{Rab7} (*alcA*^{p} driver, fructose conditions). (E) Western blot demonstrating that Thr22Asn substitution does not affect the steady-state level of GFP-RabS^{Rab7} (T22N). (F) GFP-RabS^{Rab7} (T22N) locked in the GDP conformation is cytosolic. Bars, 5 µm.

relatively devoid of these organelles. Vacuoles rarely underwent long-distance movements (Figure 3; see later discussion for a detailed consideration), making unlikely that the mechanism underlying their asymmetrical distribution involves basipetal transport. The strict and robust GFP-RabS^{Rab7} localization to vacuolar membranes facilitated time-lapse studies permitting visualization of vacuoles undergoing fusion (Supplemental Figure S1).

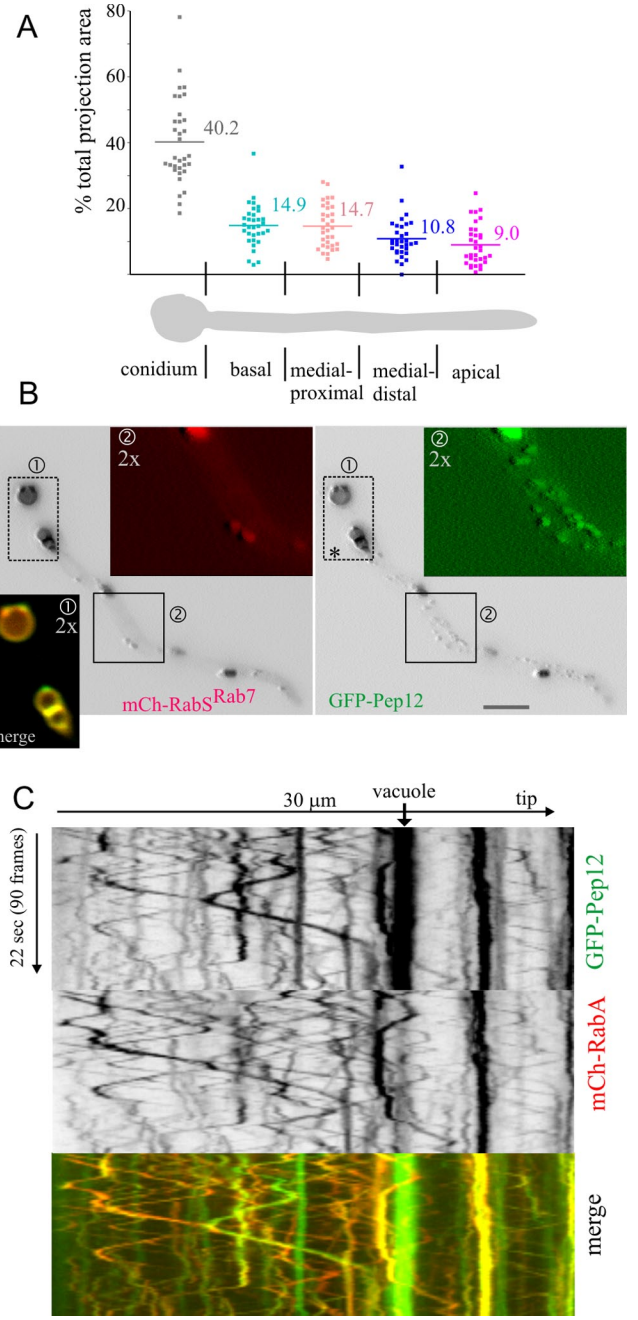

FIGURE 2: *A. nidulans* vacuolar distribution. Pep12 is present in EEs and LEs/vacuoles. (A) Vacuolar distribution: 30- to 60-µm germlings were arbitrarily divided into the "conidium" and four "rectangular" sections of approximately equivalent length, as indicated. The percentage of the total projection area occupied by vacuoles in each section was plotted in n = 33 germlings. (B) mCherry-RabS^{Rab7} colocalizes with GFP-Pep12 on vacuoles. However, GFP-Pep12 additionally localizes to punctate structures that are not labeled by mCherry-RabS^{Rab7}. Regions of interest are shown at double magnification in the indicated red, green, and merge channels. (C) Kymograph of a 4-frame/s time-lapse sequence of a cell coexpressing GFP-Pep12 and the EE marker mCherry-RabA. Pep12 and RabA colocalize in the population of rapidly moving EEs and in less abundant larger and static RabA-containing structures but not on vacuoles, which do not contain RabA.

Partial overlap of the target-SNARE Pep12 with RabS^{Rab7}

The *A. nidulans* orthologue of *S. cerevisiae* Pep12p is the only syntaxin across the endovacuolar system (Sánchez-Ferrero and Peñalva,

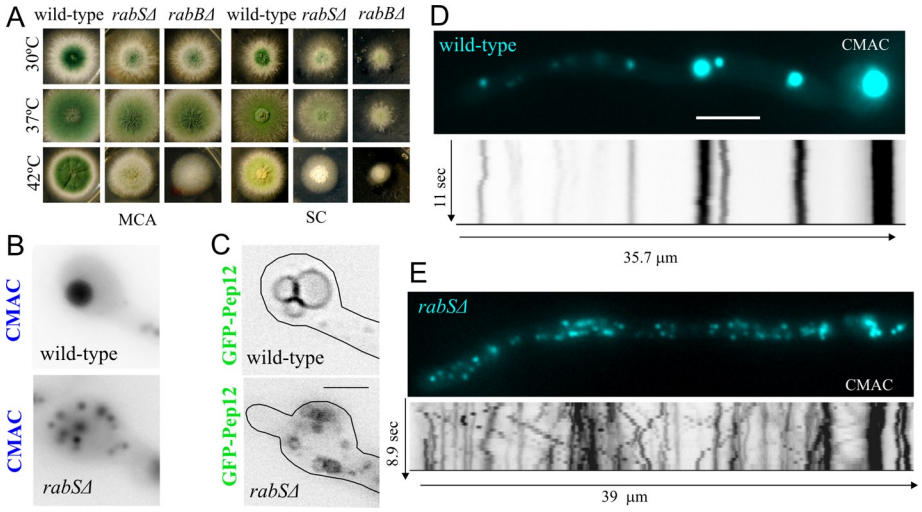

FIGURE 3: *rabS*Δ results in abnormally motile minivacuoles. (A) Growth phenotypes of the indicated strains at the indicated media and temperatures. MCA, complete medium. SC, synthetic complete medium. (B) CMAC and (C) GFP-Pep12 visualization of *rabS*Δ minivacuoles. All images are depicted at the same magnification. Bar, 2 μm. (D) Still frames (blue) and kymographs (inverted contrast, shown at the same scale as still images) correspond to 10-s time-lapse series of CMAC-stained vacuoles. Note the multiple diagonal lines seen in the *rabS*Δ example. Both images are at the same magnification. Bar, 5 μm.

2006; Findon *et al.*, 2010; *S. cerevisiae* has two—Pep12p for pre-vacuolar endosomes and Vam3p for vacuoles). mCherry-RabS^{Rab7} strictly colocalizes with GFP-Pep12, but the reverse is not true, as GFP-Pep12 labels punctate structures that do not contain RabS^{Rab7} (Figure 2B). These punctate structures undergo long-distance bidirectional movements, suggesting that they are EEs. Thus we constructed a strain coexpressing GFP-Pep12 and the EE marker mCherry-RabA and recorded time-lapse sequences (~4 frames/s) simultaneously in the GFP and mCherry channels. These sequences were analyzed with kymographs in which the *y*-axis represents the time scale. Thus static and short-range moving structures appear as vertical lines, whereas fast-moving structures appear as diagonal lines whose slope reflects the speed/direction and length reflects the range of movement of any given particle. Figure 2C shows that GFP-Pep12 localizes to static vacuoles (bright vertical lines) that do not contain RabA, to static structures containing RabA (LEs; see later discussion), and, in addition, to a population of small, bidirectionally motile structures (thus EEs; Figure 2C diagonal lines; Supplemental Movie S1) in which it colocalizes with RabA. This important finding indicates that Pep12 plays roles at the levels of the *A. nidulans* EEs, LEs, and vacuoles.

*rabS*Δ slightly impairs vegetative growth and results in a temperature-dependent defect in conidiation

We constructed a null *rabS*Δ allele, which results in a minor vegetative growth defect at any of the three temperatures tested (30, 37, and 42°C), more noticeable on synthetic than on rich medium (Figure 3A). Its most conspicuous phenotype was the nearly complete absence of conidiation at 42°C (Figure 3A). These phenotypic aspects of *rabS*Δ somewhat resemble those of *rabB*Δ (RabB is the major Rab5), but they are markedly less pronounced (Figure 3A; compare middle and right columns on SC). This indicates that RabS^{Rab7} plays a less important physiological role than RabB. The findings that *rabS*^{P}::*gfp-rabS* and *alcA*^{P}::*gfp-rabS* transgenes complement the 42°C *rabS*Δ growth and conidiation defects (demonstrating that GFP-RabS^{Rab7} is functional; Supplemental Figure S2) and that *rabS*Δ strictly cosegregates with the growth/conidiation defects in the progeny of crosses established that these phenotypic features are solely attributable to the *rabS*Δ allele.

*rabS*Δ results in proteolytically competent minivacuoles capable of undergoing movement

rabS disruption results in small vacuoles (Ohsumi *et al.*, 2002). Strains carrying *rabS*Δ indeed showed minute vacuoles (CMAC staining; Figure 3B) whose small lumen is hardly resolvable by optical microscopy (using GFP-Pep12 to label their membranes; Figure 3C). Thus, in agreement with previous data and with work in *S. cerevisiae* Ypt7p, RabS^{Rab7} is involved in the biogenesis of "normal-sized" vacuoles. *rabS*Δ "minivacuoles" show two noteworthy features: 1) They are evenly distributed across hyphae, unlike wild-type vacuoles (Figure 3, D and E), and 2) a proportion of mutant minivacuoles undergoes long-range movements similar to those of EEs (reflected by diagonal lines in kymographs), contrasting with the essentially immotile wild-type vacuoles (vertical lines in kymographs; Figure 3, D and E, and Supplemental Movies S2 [wild-type] and S3 [*rabS*Δ]). Given that the motility of EEs is RabB dependent (Abenza *et al.*, 2010), we hypothesized that the inability of endosomes to exchange RabS^{Rab7} for RabB might result in RabB persisting on minivacuoles (see later discussion).

We next determined whether *rabS*Δ minivacuoles are competent in proteolysis of an endocytic cargo, the plasma membrane amino acid permease AgtA. AgtA is expressed on glutamate medium, localizing to the plasma membrane and vacuoles (Figure 4A). If glutamate-cultured cells are shifted to ammonium, AgtA synthesis is strongly repressed, and the plasma membrane-resident pool of the transporter is delivered to the vacuole via endocytosis (Apostolaki *et al.*, 2009). In *rabS*Δ cells, AgtA-GFP is also delivered to the lumen of (mini-) vacuoles (Figure 4A). Western blots revealed similar kinetics of AgtA-GFP degradation in *rabS*Δ and *rabS*$^{+}$ cells (Figure 4B). Thus *rabS*Δ does not affect the sorting of cargoes into the MVB pathway, and minivacuoles are proteolytically competent.

RabS^{Rab7} recruits HOPS

We next used glutathione *S*-transferase (GST)–RabS^{Rab7}, loaded with GDP or GTP-γ-S, and cell extracts containing endogenously 3× hemagglutinin (HA)-tagged interactors in pull-down experiments (Figure 5A). GdiA was specifically and efficiently pulled down by GDP-loaded RabS^{Rab7}, indicating that GTP-γ-S shifts RabS^{Rab7} toward a conformation that prevents its interaction with the Rab-GDP effector GdiA (Figure 5A). The fusogenic activity of Ypt7p involves HOPS. Vps41p is the Ypt7p effector subunit in HOPS linking the complex to the GTP-loaded Rab (Cabrera *et al.*, 2010; Ostrowicz *et al.*, 2010). In agreement, *A. nidulans* Vps41 was specifically pulled down by GTP-γ-S RabS^{Rab7} but not at all by RabB, which instead pulled down Vps8 efficiently (Vps8 is the CORVET equivalent of Vps41; Peplowska *et al.*, 2007; Markgraf *et al.*, 2009). In contrast, Vps39, which also showed strict RabS^{Rab7} specificity, was preferentially retained by GTP-γ-S RabS^{Rab7} but interacted substantially with GDP-RabS^{Rab7} (Figure 5A). Given that we used unfractionated "prey extracts," this finding is consistent with the finding that whereas the Vps39-containing HOPS

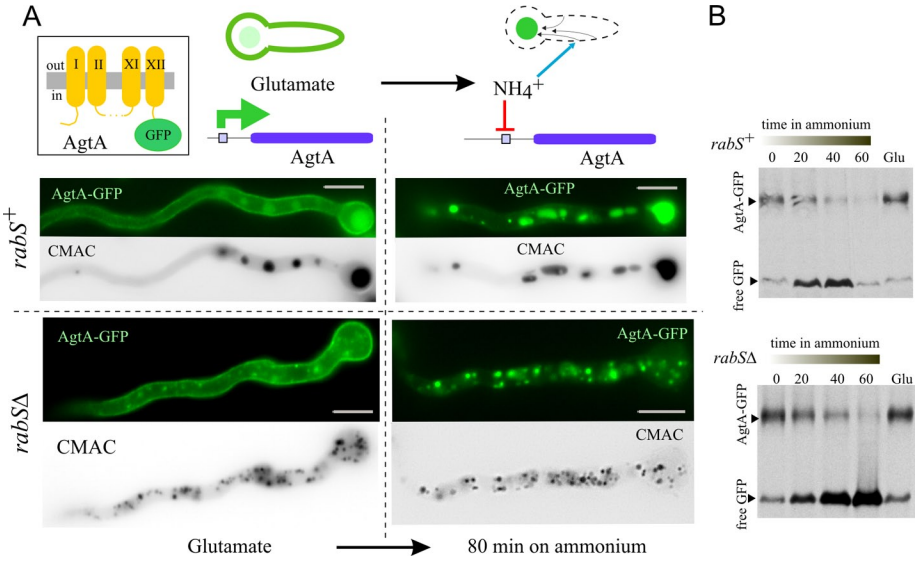

FIGURE 4: *rabSΔ* minivacuoles are proteolytically competent. (A) Normal traffic to the vacuoles of the 12-TMD protein AgtA, which mediates the uptake of dicarboxylic amino acids. In these assays, AgtA is endogenously tagged with GFP in its (cytosolic) C-terminus. Wild-type and *rabSΔ* cells expressing AgtA-GFP were initially cultured on glutamate. Under these conditions, AgtA localizes to the plasma membrane and, to a lesser extent, to the vacuoles. These cells were then shifted to ammonium, which shuts the *agtA* promoter off and promotes the endocytic delivery of plasma membrane–localizing AgtA-GFP to the vacuolar lumen. (B) Western blots showing the proteolytic vacuolar degradation of AgtA-GFP following transfer of cells to ammonium and further incubation for the indicated times. GFP is recalcitrant to degradation by vacuolar proteases but more so in the *rabSΔ* mutant.

complex is a Ypt7p (GTP) effector, "free" Vps39p binds Ypt7p irrespective of the nucleotide status (Ostrowicz *et al.*, 2010).

We passed cell-free extracts through GDP- or GTP-γ-S–loaded GST-RabS^{Rab7} affinity columns (Figure 5B). SDS–PAGE and tandem mass spectrometry (MS/MS) analyses showed that GTP-γ-S eluates contained all six components of HOPS—four components shared with CORVET (Vps11, Vps18, Vps16, and Vps33) and the HOPS-specific components Vps39 and Vps41 (Figure 5B and Supplemental Table S1). HOPS components were only slightly less efficiently retained by the GDP column, suggesting that GST-RabS^{Rab7} immobilized in the Sepharose support does not completely undergo the nucleotide-induced conformational changes mediating RabS^{Rab7} function in vivo. (Work with *S. cerevisiae* Ypt7p showed that purified HOPS shows selectivity for the GTP-γ-S–loaded Ypt7p form; Ostrowicz *et al.*, 2010.) In summary, these experiments demonstrate that HOPS is an effector of RabS^{Rab7}.

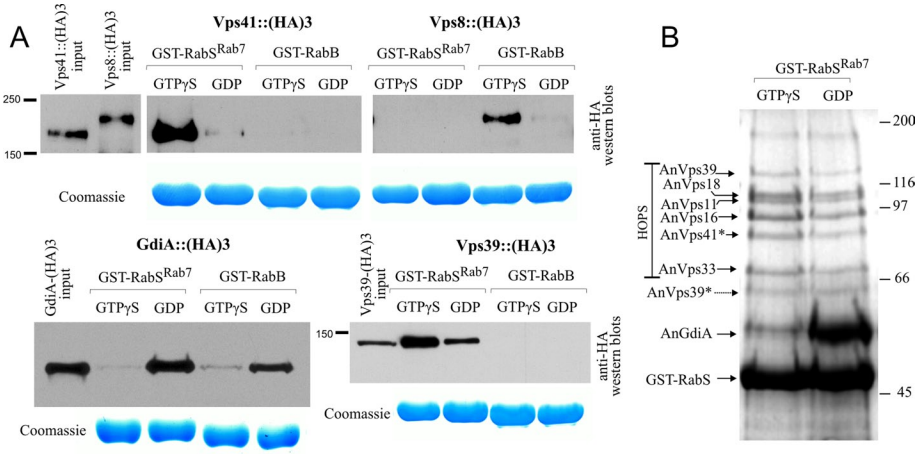

FIGURE 5: RabS^{Rab7} recruits HOPS. (A) Glutathione–Sepharose beads containing GST-RabB or GST-RabS^{Rab7} loaded with the indicated nucleotides were used as bait in pull-downs with whole-cell protein extracts, which were obtained from strains expressing, at physiological levels, GdiA (the only *A. nidulans* guanine nucleotide dissociation inhibitor), the CORVET component Vps8, or the HOPS components Vps39 and Vps41, endogenously tagged with 3× HA. The 3× HA baits were detected by Western blotting. (B) *A. nidulans* whole-cell extracts were passed through GST-RabS^{Rab7} affinity columns loaded with the indicated nucleotides, and the bound proteins were eluted, separated in an SDS–polyacrylamide gel, and stained. The identity of the bands was determined by MS/MS (Supplemental Table S1). Vps41* and Vps39** indicate that these bands are degradation products. Full-length Vps39 is also detectable in the gel.

Endosomal maturation is essential but vacuolar fusion is not

The two Rab5s (RabA and RabB) and their effectors mediate the coalescence of EEs and their maturation into LEs (Abenza *et al.*, 2010). Vps45 and its binding partner Vac1^{Vps19} are specific RabB effectors, whereas the CORVET complex (containing Vps8) is a RabB and RabA effector (Abenza *et al.*, 2010). A double *rabAΔ rabBΔ* deletion is nearly lethal, and single *vps45Δ* and *vps8Δ* mutations are severely debilitating (Abenza *et al.*, 2010), as are deletions involving ESCRT-0, -I, -II, and -III components mediating the biogenesis of multivesicular endosomes (Calcagno-Pizarelli *et al.*, 2011). These data indicate that maturation and coalescence of EEs into larger structures (LEs) is essential. In contrast, *rabSΔ* mutants are perfectly viable, and thus the RabS^{Rab7}-mediated fusion of LEs with vacuoles, of LEs with LEs to form vacuoles, and the homotypic fusion of vacuoles is largely dispensable (Figure 3A).

These conclusions led to three predictions: 1) *vac1Δ* should be as severely debilitating as *vps45Δ*; 2) deletion of any one gene encoding a HOPS class C component shared with CORVET should lead to near lethality due to its role in CORVET; and 3) deletion of the gene encoding the HOPS-specific subunit Vps41 should be viable, phenocopying *rabSΔ* mutations. We deleted *vac1* and *vps18* (Vps18 is a class C CORVET and HOPS subunit). Figure 6A shows the corresponding growth phenotypes. *vac1Δ* colonies show severely reduced growth, similar to that of *vps45Δ* colonies. The growth defect of *vps18Δ* colonies is even more marked, indicating that this class C protein is virtually essential.

Vps41 is the HOPS equivalent of CORVET Vps8 (Peplowska *et al.*, 2007). In marked contrast with *vps8Δ* or *vps18Δ*, *vps41Δ* strains are relatively healthy and indistinguishable from a *rabSΔ* strains in growth and conidiation (note the slight reduction in

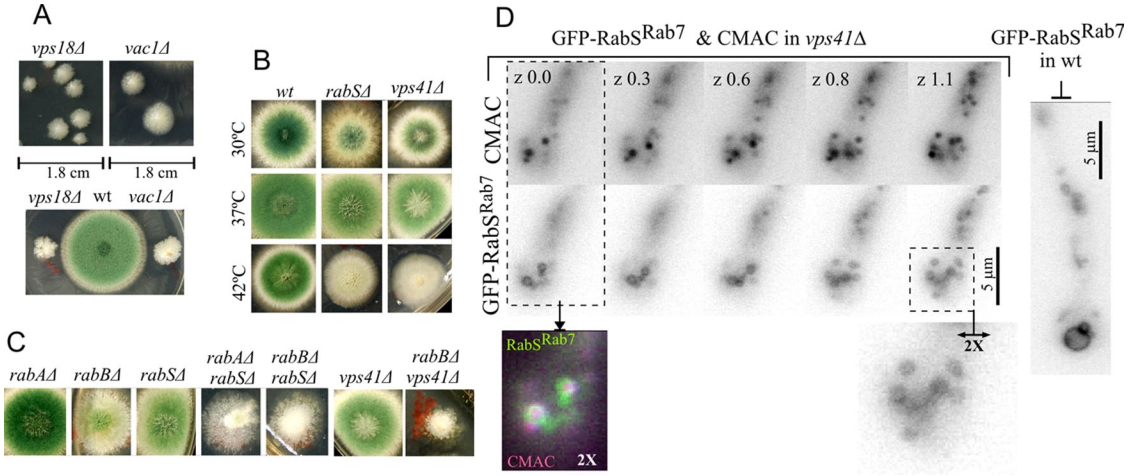

FIGURE 6: Genetic studies of endosomal maturation. (A) Growth phenotypes of *vps18*Δ (encoding a class C subunit shared by the CORVET and HOPS complexes) and *vac1*Δ (Vac1, also denoted Vps19, is a specific RabB effector). *vps18*Δ and *vac1*Δ are very severely debilitating. Note that *vps18* was previously called *digA*. A *digA1* early-truncating mutation removing the Vps18 C-terminal RING finger leads to a temperature-dependent growth defect (Geissenhoner *et al.*, 2001). (B) Growth phenotypes at the indicated temperatures of *vps41*Δ compared with *rabS*Δ. The two mutations are phenotypically indistinguishable. (C) Both *rabA*Δ and *rabB*Δ result in a synthetic growth defect in double mutants with *rabS*Δ. *rabB*Δ also results in a similar synthetic growth defect in double mutants with *vps41*Δ (*rabA*Δ was not tested in combination with *vps41*Δ). (D) Like *rabS*Δ, *vps41*Δ results in minivacuoles. In the absence of Vps41, the limiting membranes of CMAC-containing minivacuoles are labeled with GFP-RabS^{Rab7}. Images of a *z*-series are shown, with numbers indicating relative *z*-position in micrometers. For comparison, GFP-RabS^{Rab7} wild-type vacuoles are shown on the right.

colony size and lack of conidiation at 42°C; Figure 6B). CMAC staining (Supplemental Figure S3) showed that *vps41*Δ mutants also resemble *rabS*Δ mutants in the "minute vacuole" phenotype and in the loss of the tip-to-base gradient of vacuolar distribution. Thus the *rabS*Δ minute vacuole phenotype results from inability to recruit HOPS. Vps41, able to bind membranes of LEs via its ALPS domain (Cabrera *et al.*, 2010), might conceivably contribute to the membrane recruitment of its Rab. However, GFP-RabS^{Rab7} is recruited to the membranes of CMAC-stained *vps41*Δ minivacuoles in the absence of Vps41 (Figure 6D).

The motility of the *rabS*Δ minivacuoles suggests that they retain endosome features, even though they have the characteristic spherical shape of vacuoles and their lumen is large enough to be optically resolvable. However, in the absence of RabS^{Rab7} (and therefore of HOPS), endosomes can only fuse into minivacuoles by using CORVET (i.e., in a RabA/RabB-dependent manner; Abenza *et al.*, 2010).

*rabB*Δ and *rabA*Δ are synthetically sick with *rabS*Δ, the double mutations leading to a stronger impairment of growth and conidiation than either single deletion (Figure 6C). Given that *vps41*Δ and *rabS*Δ cause similar synthetic growth defects in combination with *rabB*Δ (Figure 6C), the debilitating effect of the double *rabS*Δ *rabB*Δ mutation involves the inability to recruit HOPS and not another RabS^{Rab7}-mediated process. Two non–mutually exclusive interpretations can account for these observations. One is that in the absence of RabS^{Rab7}/HOPS, impairing the recruitment of CORVET to endosomes critically compromises the formation of functional *rabS*Δ minivacuoles. A second is that RabS^{Rab7}/HOPS has RabA/RabB-independent functions. For example, *rabS*Δ could prevent, in addition to LE–vacuole and vacuole–vacuole fusion, the entry of Vps41-dependent traffic into the vacuoles through a pathway akin to the *S. cerevisiae* AP-3 pathway (Cabrera *et al.*, 2010).

Subcellular distribution of Rab5s and RabS^{Rab7}

To study endosomal Rab transitions, we constructed strains expressing mCherry-RabS^{Rab7} and GFP-RabA or GFP-RabB from single-copy *alcA^{p}*-driven transgenes. Using this regulatable (by the carbon source) promoter allowed us exploit three different levels of expression: low (fructose), intermediate (glycerol), and high (ethanol). None of these carbon source conditions led to any detectable effect on colony growth (Supplemental Figure S4), strongly indicating that expression of the fusion proteins does not interfere with the physiology of the endosomal system.

We acquired high-speed time-lapse sequences (10–20 frames/s) of these strains in the red and green channels simultaneously using a Dual-Viewer. RabS^{Rab7} and RabA/RabB showed little colocalization (Figure 7A and Supplemental Movies S4 and S5). RabS^{Rab7} localized to the vacuolar membranes, to relatively static structures, and, occasionally, to moving structures (see later discussion). By contrast, RabA or RabB did not label the vacuolar membranes at all, localizing to moving EEs and to less abundant static structures. As in *U. maydis* (Schuster *et al.*, 2011), moving RabA/RabB EEs usually traveled for several seconds in one direction before reversing movement in the opposite direction, with (U-shaped tracing in the kymograph; Figure 7B) or without (V-shaped tracings; Figure 8) arresting for some time in between. This behavior reflects the tug-of-war action of dynein and kinesins on the same endosome (Schuster *et al.*, 2011). Time-lapse sequences revealed very unusual examples of vacuolar movement, like the ~6-µm journey of the small vacuole in Figure 7C to dock at a large vacuole (Supplemental Movie S6). This movement was short ranged and slower than that of EEs (compare slopes of green- and red-channel kymographs).

The transition between RabA/RabB and RabS^{Rab7} is sharp

RabB is the major determinant of endosomal maturation (Abenza *et al.*, 2010). Fructose kymographs (Figure 8, A1 and A2) revealed occasional yet rare examples of moving GFP-RabB EEs faintly stained with mCherry-RabS^{Rab7} (Figure 8A2, arrows). In contrast, static structures containing RabB and RabS^{Rab7} were clearly more abundant (Figure 8A1, arrows). Similar overall absence of colocalization in moving structures was seen on glycerol, despite the increased

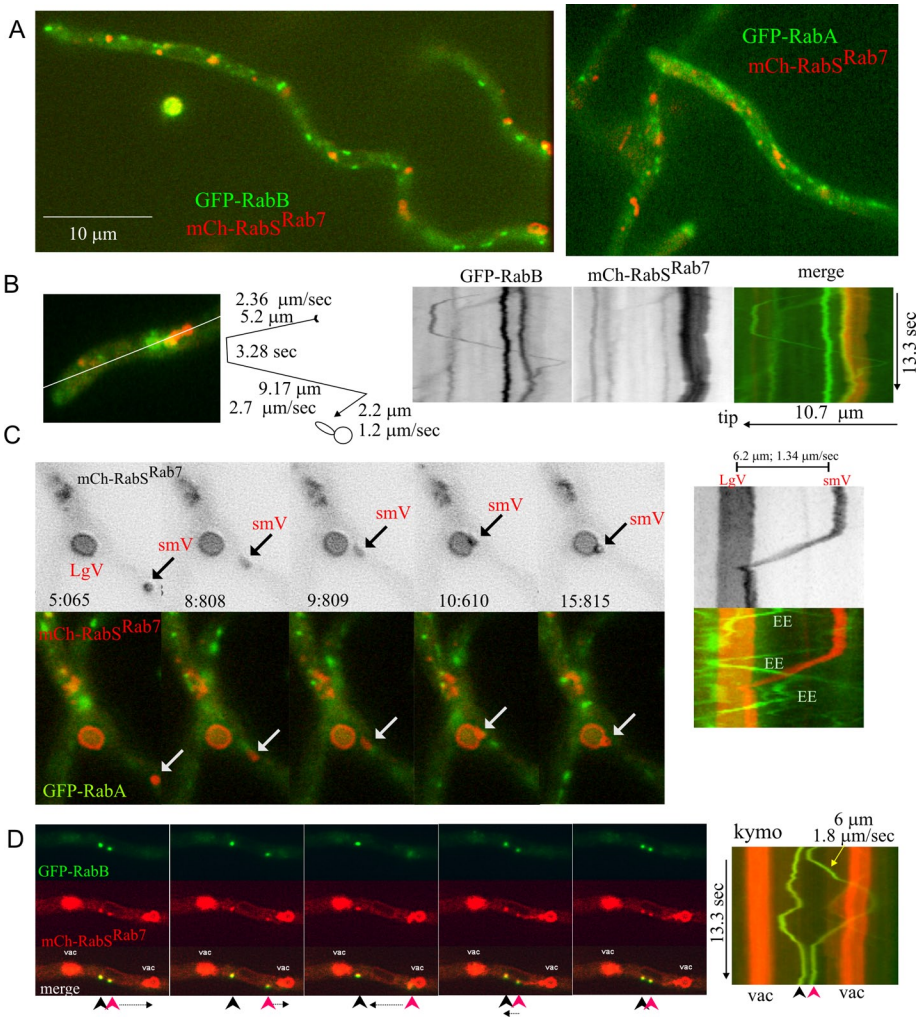

FIGURE 7: Coimaging of early endosomal Rabs and RabS^{Rab7}. (A) Still frames showing that RabS^{Rab7} and RabB or RabA show little colocalization. (B) Examples of static and moving endosomes: RabB (green) and RabS^{Rab7} (mCherry). A kymograph was plotted across the indicated line. Three static RabB endosomes, one moving EE, and two small vacuoles strongly labeled with RabS^{Rab7}are shown. The tip-distal static RabB endosome is docked at the most anterior RabS^{Rab7} vacuole (yellow in the channel merge). The movement of a fourth RabB endosome is schematically represented. (C) One example (arrows) of a basipetally moving small RabS^{Rab7} vacuole (smV) that docks against a large vacuole (LgV). Kymographs on the right depict how the speed (diagonal slope, 1.34 µm/s) of this moving vacuole is markedly lower than that of RabA endosomes. See Supplemental Movie S6. (D) RabB and RabS^{Rab7} can coexist on LEs: two LEs containing RabB and RabS^{Rab7}, located between two vacuoles. One of the endosomes moves in one direction before shifting toward the opposite direction, but its speed (1.8 µm/s) is lower than the average speed of EEs. Frames correspond to supplemental Movie S7.

fluorescence signal. Again, colocalization predominated in the more static structures or in those motile structures that moved for shorter distances and at slower speeds than EEs (Supplemental Figure S5A). Figure 7D and Supplemental Movies S7 and S8 show structures containing RabB and RabS^{Rab7} moving at 1–1.8 µm/s, more slowly than EEs (~2.5 µm/s; Abenza *et al.*, 2009). We speculate that these double-labeled structures, whose size would impede/retard movement, represent late or mature endosomes where Rab conversion is taking place.

To confirm that RabB and RabS^{Rab7} can actually coincide on the less motile endosomes, we induced the transgenes with ethanol, which results in strong overexpression of the Rabs. RabB still localized to fast-moving EEs. It also localized to aggregates that, albeit motile, generally moved for shorter distances (Figure 8, B1 and B2). RabS^{Rab7} was clearly present in a proportion of RabB-containing structures, generally corresponding to these large aggregates (Figure 8, B1 and B2, double arrowed; one "control" RabS^{Rab7}-negative EE is single arrowed). However, RabB was absent from vacuolar membranes, even though these were strongly positive for RabS^{Rab7}. Therefore, although these strongly overexpressing conditions are not physiological, these experiments establish that RabS^{Rab7} can be recruited to endosomal membranes containing high levels of RabB. In contrast, RabB is excluded from vacuolar membranes, where RabS^{Rab7} is abundant. These data are consistent with a maturation model in which endosomes acquire RabS^{Rab7} in their late steps of maturation, losing RabB as they become vacuoles.

Similar experiments using GFP-RabA revealed a previously unnoticed feature of RabA endosomes: even under fructose conditions leading to GFP-RabA levels similar to those attained with the endogenous promoter (Abenza *et al.*, 2009), we detected a background of very abundant small, moving endosomes that we did not see with GFP-RabB; their kymograph tracings formed a net of diagonal lines against which vertical lines of more static aggregates were prominent (Figure 8, C and D, Supplemental Figure S5, and Supplemental Movie S9). As with RabB, we only very occasionally detected EEs labeled with RabS^{Rab7} and RabA. The tracings arrowed in Figure 8D and Supplemental Figure S5B are the only examples among the numerous moving RabA EEs in which RabS^{Rab7} was detectable. We thus conclude that the transition between RabA/RabB and RabS^{Rab7} domains is relatively sharp.

RabB and RabA reach the vacuoles in *rabSΔ*

rabSΔ markedly increases the abundance of RabA/RabB structures. In 30-µm-long projections of wild-type tip regions (n = 8 hyphae), GFP-RabB structures accounted for 4.4 ± 0.6% of the area. This figure was markedly higher (sixfold; 23.3 ± 2.5%) in the mutant. This hypertrophy of the *rabSΔ* endosomal compartment might reflect the inability of LEs to undergo HOPS-mediated fusion or the ability of EE Rabs to invade membranes otherwise restricted to RabS^{Rab7} (or both). One observation lent credence to the "Rab5 invasion" possibility. In the wild type, GFP-RabA/RabB eventually label aggregates of endosomes that are not vacuoles (they are multivesicular, irregularly shaped, and CMAC negative; Abenza *et al.*, 2009, 2010; Griffith *et al.*, 2011). In contrast, in *rabSΔ* cells, both RabA (Supplemental Movie S10) and RabB (Figure 9A) clearly label the membranes of minivacuoles. To further demonstrate this, cells expressing GFP-RabB were pretreated with benomyl (to abolish the microtubule [MT]-dependent motility of minivacuoles)

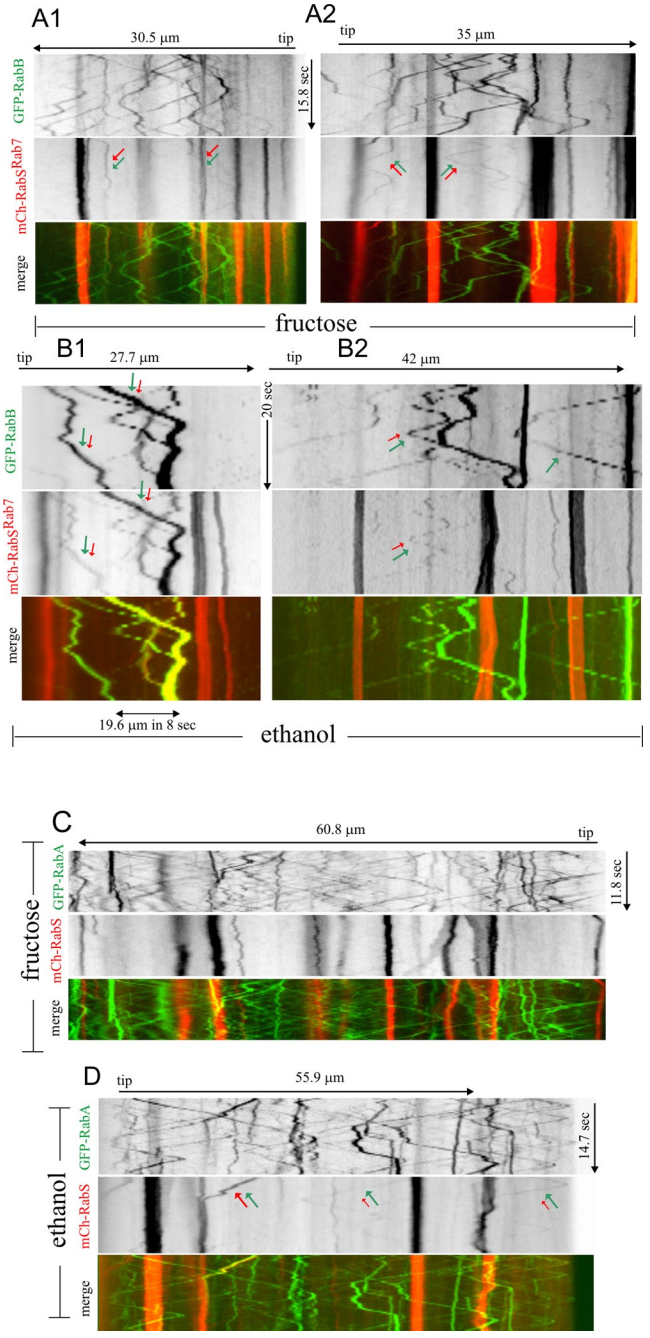

FIGURE 8: Kymographs of "stream" time-lapse series of GFP-labeled Rab5s and mCherry-RabS^{Rab7}. Images in the GFP (Rab5s) and mCherry (RabS^{Rab7}) channels were simultaneously acquired using a Dual-View beam splitter with "stream" acquisition, a routine by which images are directly discharged from the camera chip to the computer RAM memory at maximal speed. The resulting time series were used to draw kymographs. All kymographs, whose time and length dimensions are indicated, are displayed to the same scale and are thus directly comparable. (A, B) GFP-RabB and (C, D) GFP-RabA, as indicated. Expression of all three fluorescent fusion proteins was governed by the regulatable *alcA*^{p} driver and thus can be manipulated by the carbon source in the medium. All transgenes were integrated in single copy into known chromosomal locations. For GFP-RabB: (A1) Arrows show two static endosomes containing RabB and mCherry-RabS^{Rab7}. (A2) Arrows show two rare examples of moving endosomes containing RabB and RabS^{Rab7}. (B1, B2) Strongly overexpressing conditions. Examples of moving endosomes containing RabB and mCherry-RabS^{Rab7} are indicated with red and green arrows. (B2) One RabB endosome that does not contain mCherry-RabS^{Rab7} is indicated with a single green arrow. GFP-RabA: (C) Virtually no colocalization of GFP-RabA and mCherry-RabS^{Rab7} is seen in the numerous examples of moving endosomes detected across this 60-µm-long region. (D) The endosome on the left (red and green arrows of equal size), containing GFP-RabA and mCherry-RabS^{Rab7}, moves toward the tip until it docks at a LE/vacuole. Two examples of GFP-RabA moving endosomes faintly stained with mCherry-RabS^{Rab7} are indicated with green (large) and red (small) arrows. Note that moving RabA structures (diagonals in C and D) are clearly more numerous than moving RabB structures (A and B).

and loaded with CMAC. Whereas hardly any overlap of RabB with CMAC was detectable in the wild type, most RabB-containing structures in the *rabS*Δ mutant were CMAC positive (Figure 9B). Because vacuolar membrane labeling by RabA/RabB is never seen in the wild type, these data suggest that displacement of RabA/RabB from EEs once they reach the LE stage requires RabS^{Rab7}.

We next tested whether GFP-RabS^{Rab7} localization to vacuoles necessitates RabB. GFP-RabS^{Rab7} is recruited to the membrane of *rabB*Δ vacuoles, although clearly less efficiently than in the wild type (Figure 9C). This finding is consistent with the interpretation that the vacuolar RabS^{Rab7} localization involves CORVET, as RabA is also able to recruit CORVET to endosomes, albeit less efficiently than RabB (note that lethality-causing *rabA*Δ *rabB*Δ double deletion cannot be tested).

The role of dynein-mediated basipetal movement in endosomal maturation

Given that the amount and size of vacuoles increase with the distance to the tip, we hypothesized that maturation of endosomes into vacuoles might be coupled to the dynein-mediated movement of endosomes away from the tip (MTs are oriented with their plus ends toward the apex). Thus, if dynein function is compromised, EEs would be expected to mature in the proximity of the tips. Indeed the dynein (heavy chain) *nudA1*^{ts} mutation caused a pronounced effect on the apicobasal distribution of GFP-RabS^{Rab7}–labeled vacuoles. In *nudA1*^{ts} germlings (Figure 10A) and hyphae (Figure 10B) there was a marked accumulation of vacuoles near the tip that was never seen in the wild type (wild-type tip-proximal regions are actually devoid of vacuoles). Clusters of *nudA1*^{ts} vacuoles did not invade the actual tip of hyphae (Figure 10B). These findings strongly support a model according to which endosomes mature to LEs that become engaged in homotypic fusion events to coalesce into larger vacuoles as they move away from the tip (Figure 11). We also constructed *nudA1 rabB*Δ double-mutant strains expressing GFP-RabS^{Rab7}. This double mutation does not prevent the vacuolar localization of RabS^{Rab7} (as noted, RabA is able to recruit CORVET), even though these strains display the characteristic *nudA1* accumulation of vacuoles near the tip (Supplemental Figure S6B).

We conducted additional experiments using CMAC to visualize vacuoles in cells that do not express any fluorescent Rab. *nudA1* hyphal tip cells indeed accumulate clusters of small vacuoles within the apicalmost 10- to 20-µm region. These clusters were absent in the wild type (Figure 10, D and E), in agreement with data presented earlier. We also noticed that in *rabS*Δ cells, the otherwise ubiquitous minivacuoles are absent from the tip (Figure 10, D and E), suggesting that they are excluded from this region, predictably by dynein-mediated transport. If this were true, in *nudA1*^{ts} cells minivacuoles should invade the tip, forming a minivacuolar analogue of the EE cluster characteristic of dynein-deficient hyphal tips (Lenz *et al.*,

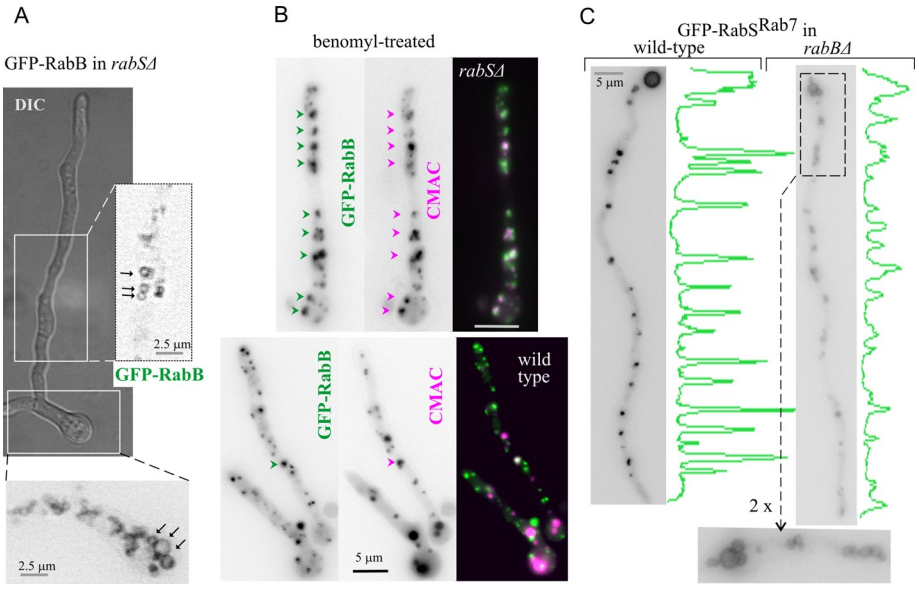

FIGURE 9: In *rabS*Δ strains, RabB invades vacuolar membrane domains normally occupied by RabS^{Rab7}. (A) GFP-RabB in *rabS*Δ. Inverted contrast images correspond (at double magnification) to the indicated regions of interest in the Nomarski panel. They show how the early endosomal RabB reaches the membrane of *rabS*Δ minivacuoles. Similar data obtained for GFP-RabA are displayed in Supplemental Movie S10. (B) Microtubules were depolymerized with benomyl. Under such conditions, endosomes form aggregates. In the wild type, endosomal aggregates show little colocalization with CMAC-stained LEs/vacuoles (one colocalizing particle is shown by the arrow). In contrast, colocalization is very conspicuous in the *rabS*Δ mutant, strongly indicating that CMAC-stained *rabS*Δ minivacuoles retain early endosomal identity. (C) In *rabB*Δ cells, GFP-RabS^{Rab7} localizes to the vacuolar membranes but less efficiently than in the wild type. The relative difference of fluorescence is illustrated by the line scans on the right. The inset below the *rabB*Δ cell shows the faint yet clear labeling of vacuolar membranes.

2006; Zekert and Fischer, 2008; Abenza *et al.*, 2009). This is indeed the case (Figure 10, D and E). Double-mutant *nudA1^{ts} rabS*Δ cells accumulate most of their minivacuoles at and near the tip, with the rest of the cell largely devoid of them. Invasion of *nudA1^{ts}* tip regions by minivacuoles is very conspicuous in young branches (Supplemental Figure S6A).

Finally, we hypothesized that by impairing EE movement, *nudA1* would confine maturation of EEs into LEs/vacuoles within the tip. Thus we examined *nudA1* cells coexpressing fluorescent RabB and RabS^{Rab7} that had been shifted to the restrictive temperature for 4 h. These cells contained the characteristic *nudA1* aggregate of RabB-containing endosomes unable to depart from the tip (Figure 10C) and the also characteristic tip-proximal clusters of RabS^{Rab7} vacuolar structures. RabB aggregates and RabS^{Rab7} structures were very closely associated and showed partial colocalization (Figure 10C and Supplemental Figure S7). However, in every example analyzed (n = 47 tips examined with Dual-Viewer *z*-stacks), the cluster of LE/vacuolar structures was less apical or, at most, overlapped with the EE aggregate (Supplemental Figure S7), strongly supporting the view that conversion of RabB EEs into RabS^{Rab7} LEs/vacuoles is coupled to basipetal movement of the former.

DISCUSSION

In *U. maydis* and *A. nidulans* kinesin-3 and dynein mediate the long-distance movement of EEs (Wedlich-Soldner *et al.*, 2002; Lenz *et al.*, 2006; Zekert and Fischer, 2008; Abenza *et al.*, 2009, 2010). Endocytosis predominates in the tip region (Araujo-Bazán *et al.*, 2008; Taheri-Talesh *et al.*, 2008), which is the major source of EEs (Figure 11). These endosomes move away from the tip using dynein. Thus, in *A. nidulans* strains deficient in the NudA dynein, in the dynein activator NudF, in the KinA kinesin-1 transporting dynein to MT plus ends, or in the dynactin p25 subunit linking EEs to dynein, EEs aggregate in the tips (Zekert and Fischer, 2008; Abenza *et al.*, 2009; Zhang *et al.*, 2010, 2011).

In time-course experiments, the endocytic tracer FM4-64 arrives first to motile EEs and, in a posterior stage, to a population of larger, static LEs (Peñalva, 2005; Hervás-Aguilar *et al.*, 2010). Thus the transition from EE to LEs takes place with simultaneous loss of motility. In our model, maturation of EEs is coupled to their movement away from the tip (Figure 11), resembling the situation in mammalian cells, in which Rab5 EEs that form in the cell periphery (the hyphal tip equivalent) move centripetally (i.e., basipetally in fungal hyphae) on dynein while they augment their size (Rink *et al.*, 2005). However, in mammalian cells, LEs/lysosomes also undergo dynein-mediated centripetal transport toward the minus ends of MTs. Recruitment of dynein-dynactin to LEs/lysosomes is mediated by the Rab7 effector RILP (Jordens *et al.*, 2001). RILP homologues are absent from fungi. Thus inefficient dynein recruitment might contribute to the reduced motility of *A. nidulans* LEs enriched in RabS^{Rab7}.

Our model in Figure 11 accounts for the observations that tip-proximal regions contain very few vacuoles (the end product of endosomal maturation) and that vacuolar size increases with the distance to the tip. It is strongly supported by three findings: 1) Vacuoles accumulate near the tip region of *nudA1^{ts}* cells; 2) unlike wild-type vacuoles, *rabS*Δ minivacuoles, which are abnormally motile, are uniformly dispersed across the cytosol; and 3) In *nudA1^{ts}* cells, overlap of Rab5 and RabS^{Rab7} membranes is detectable in the tip, suggesting that if retrograde EE movement is prevented, endosomes mature on the spot.

The absence of RabS^{Rab7} prevents the formation of normal-sized vacuoles. The resulting minivacuoles have features of EEs: 1) They are able to eventually undergo long-distance movement; 2) they invade the apicalmost regions of *nudA1^{ts}* tips, resembling EEs; and 3) they contain EE Rabs on their membranes. The finding that Rab5s invade LE/vacuolar membranes only if RabS^{Rab7} is absent is consistent with the models in which maturation of EEs into LEs/vacuoles occurs by Rab conversion (Rink *et al.*, 2005; Peplowska *et al.*, 2007; Brocker *et al.*, 2010). In a simplified model, this implies that Rab5/CORVET membrane domains are converted into Rab7/HOPS domains (Rink *et al.*, 2005). A key regulator of this conversion is a complex of two proteins formed by Mon1p/Ccz1p in *S. cerevisiae* (Nordmann *et al.*, 2010) and SAND-1/CCZ-1 in *C. elegans* (Kinchen and Ravichandran, 2010). The findings that SAND-1/CCZ-1 is itself a Rab5 effector (Kinchen and Ravichandran, 2010), that the localization to endosomes of Mon1p/Ccz1p is Vps21p (Rab5) and CORVET dependent (Nordmann *et al.*, 2010), that the complex interacts with HOPS components (Nordmann *et al.*, 2010; Poteryaev *et al.*, 2010), and, of importance, that Mon1p/Ccz1p is the guanine nucleotide exchange factor (GEF) of

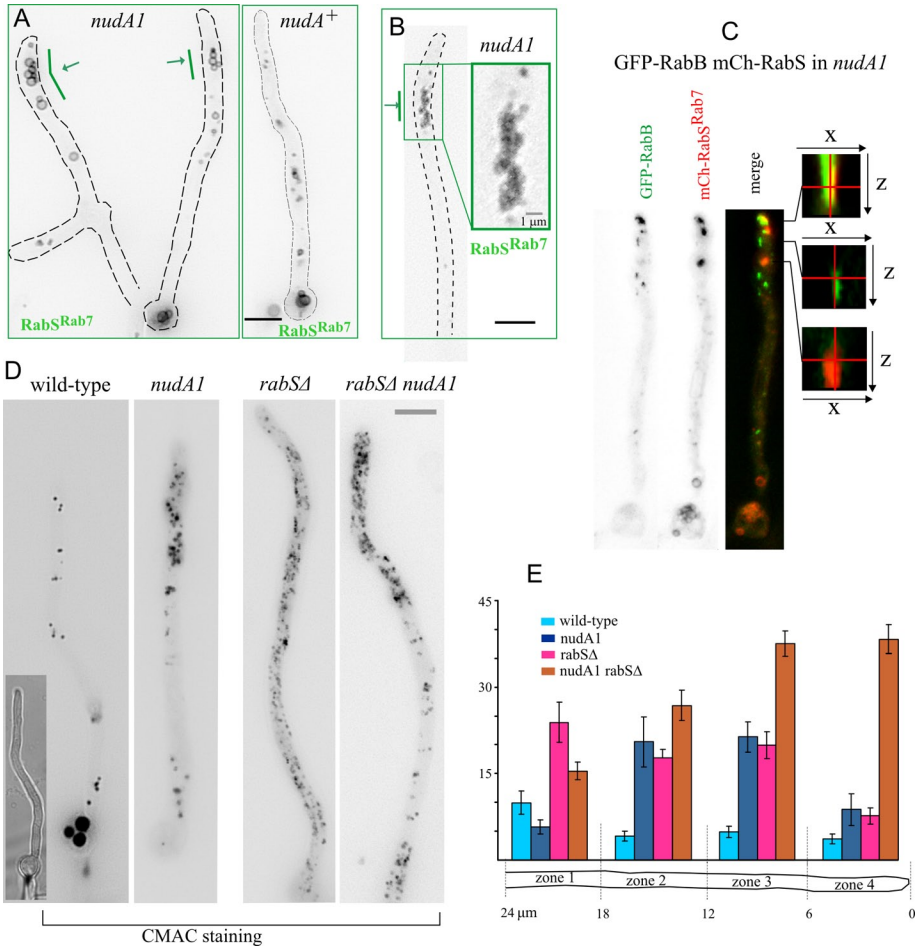

FIGURE 10: *nudA1*^{ts} results in the accumulation of vacuoles near the tip. (A) *nudA1*^{ts} and control wild-type germlings and (B) a *nudA1* hyphal tip expressing GFP-RabS^{Rab7} under the control of the *alcA*^{p} driver. In both cases cells were cultured at 37°C. (C) GFP-RabB and mCherry-RabS^{Rab7} colocalize in tip aggregates of *nudA1*^{ts} cells cultured on fructose. Shown are *x*-*z* orthogonal views of *z*-stacks in the positions of aggregates containing mCherry-RabS^{Rab7} only (red, bottom), GFP-RabB only (green, middle), or both (top). In the latter, the overlap across several *z*-planes of red and green signals shows that RabB and RabS^{Rab7} membranes overlap. (D) Accumulation of CMAC-stained vacuoles near the tip of *nudA1*^{ts} and *nudA1*^{ts} *rabS*Δ cells. Note that, in the *nudA1*^{ts} *rabS*Δ cell, CMAC minivacuoles invade the hyphal tip. (E) Quantification of the surface occupied by CMAC-stained structures in the different mutant conditions shown in D. Hyphal tip cells were segmented into four 6-µm-long regions as indicated.

Ypt7p (yeast Rab7) provide the mechanistic bases for the Rab5-to-Rab7 conversion: Rab5 recruits Mon1/Ccz1, then Mon1/Ccz1 activates Rab7, and the GEF is further stabilized by Rab7 effectors. Mon1/Ccz1 influences Rab5 localization (Nordmann *et al.*, 2010). Given that *C. elegans* SAND-1 displaces the Rab5 GEF from membranes (Poteryaev *et al.*, 2010), fungal Mon1/Ccz1 could plausibly act in a similar manner. The relatively sharp Rab transition that we observe is indeed consistent with this possibility. Moreover, the finding that, in the absence of RabS^{Rab7}, Rab5s (RabA/RabB) reach the vacuolar membranes suggests that RabS^{Rab7} contributes to destabilizing the association of Rab5s with membranes (Figure 11).

Our data strongly indicate that the transition between Rab5s and RabS^{Rab7} is sharp, as examples of rapidly moving RabA/RabB EEs that also contain RabS^{Rab7} are very rare. Inspection of a large number of movies taken under a variety of conditions revealed that colocalization of RabA/B and RabS^{Rab7} is relatively frequent in static or short-range moving particles or in large particles that move at speeds considerably below the average speed of EEs, most likely representing LEs whose mobility is constrained by their size. Thus RabS^{Rab7} is recruited to membranes already at the level of LEs and it is not confined to vacuoles, in agreement with data in *S. cerevisiae* (Balderhaar *et al.*, 2010). In contrast, RabA or RabB, both of which reside in EEs, can reach LEs but are normally absent from vacuoles.

Fusion of *A. nidulans* LEs with vacuoles and among vacuoles themselves is dispensable, as demonstrated by the relatively mild growth defects resulting from *rabS*Δ, *vps41*Δ (this work) and *vps39*Δ (Oka *et al.*, 2004). In contrast, double *rabA*Δ *rabB*Δ deletion is lethal (Abenza *et al.*, 2010), and single deletion of each tested gene involved in maturation of EEs into LEs is very severely debilitating. Tested mutations include *vps45*Δ, *vps8*Δ (CORVET; Abenza *et al.*, 2010), *vps18*Δ and *vac1*Δ (this work), ESCRTΔ alleles (single *vps27*Δ, *vps23*Δ, *vps20*Δ, *vps24*Δ, and *vps32*Δ mutations), and a conditional expression allele of Vps4 (Rodríguez-Galán *et al.*, 2009; Calcagno-Pizarelli *et al.*, 2011; Galindo *et al.*, 2012). Of note, the severely debilitating effect of ESCRTΔ alleles is suppressible by loss-of-function mutations in the filamentous fungal–specific *sltA* gene regulating cation homeostasis (Findon *et al.*, 2010; Calcagno-Pizarelli *et al.*, 2011), suggesting that the essential role of endosomal maturation might be related to cation homeostasis

*rabS*Δ minivacuoles are proteolytically competent and contain Pep12. Thus resident proteases or Pep12 must be able to reach vacuoles through endosomes, because the direct AP-3 pathway to the vacuole requires Ypt7p/HOPS/Vps41p (Angers and Merz, 2009; Cabrera *et al.*, 2010). In the absence of RabS^{Rab7}, the formation of minivacuoles possibly occurs through the CORVET-mediated homotypic fusion of endosomes (Markgraf *et al.*, 2009), but CORVET alone appears to be insufficient to sustain further enlargement of minivacuoles. Thus an attractive and as yet untested possibility is that CORVET and HOPS complexes mediate homotypic fusion events but that these events involve partners with different degrees of membrane curvature, depending on the Rab/tether combination.

MATERIALS AND METHODS

Aspergillus media and molecular biology

Synthetic complete medium (SC; Cove, 1966) contained 1% glucose and 5 mM ammonium tartrate unless otherwise indicated. Complete medium for *Aspergillus* (MCA) was used for strain maintenance. Strains are listed in Supplemental Table S2 (*vps18*Δ, *Vac1*Δ, and the double mutants *rabA*Δ-*rabS*Δ, *rabB*Δ-*rabS*Δ, and *vps41*Δ-*rabB*Δ strains were impossible to keep beyond the described experiments due to their severely debilitated phenotype). For growth tests involving different carbon sources, we cultivated the strains on SC containing 5 mM ammonium tartrate and 3% glucose,

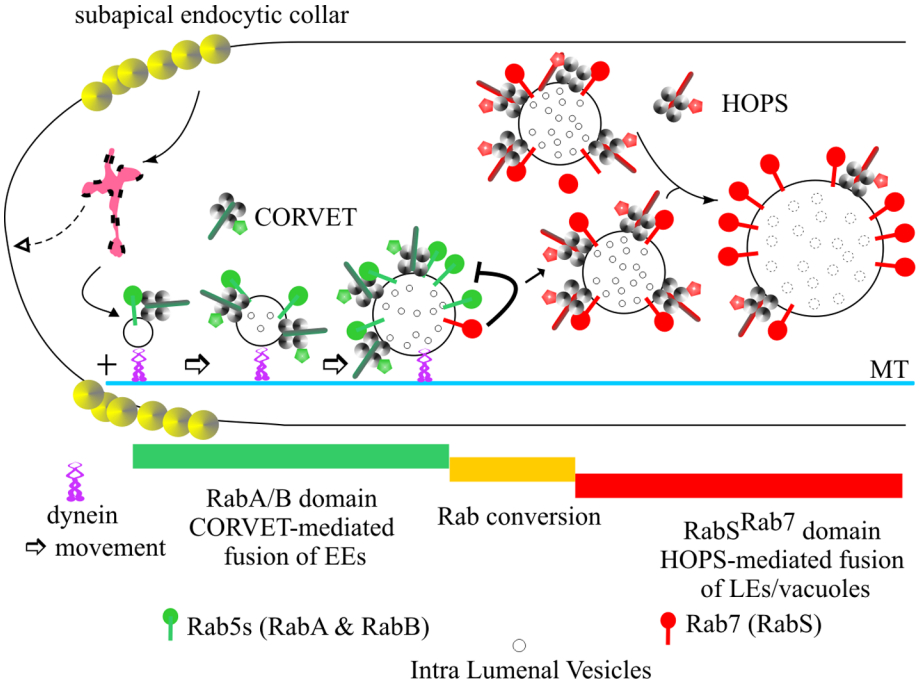

FIGURE 11: A model for endosomal maturation in *A. nidulans*. This model for endosomal maturation incorporates the conclusions of this work into the interpretation of the endocytic pathway derived from previous reports (Ohsumi *et al.*, 2002; Peñalva, 2005; Abenza *et al.*, 2009, 2010; Hervás-Aguilar and Peñalva, 2010; Hervás-Aguilar *et al.*, 2010; Zhang *et al.*, 2010, 2011; Griffith *et al.*, 2011; Pantazopoulou and Peñalva, 2011). Endocytosis predominates in the tip. Endocytic vesicles reach a hypothetical endosomal compartment that would act as a sorting endosome, organized as a mosaic of domains (magenta). We speculate that this mosaic includes domains from which membrane and cargo can recycle to the plasma membrane, segregating from other domains in which the two Rab5s—RabA and RabB—determine "degradative" EE identity (i.e., specify the identity of membranes destined to the vacuole). It is generally accepted that efficient endocytic recycling is required for hyphal morphogenesis. Thus the hypothetical existence of a sorting endosome acting upstream of RabB is supported by the fact that *rabB*Δ has a relatively minor effect on hyphal morphogenesis (Abenza *et al.*, 2010). Degradative EEs become loaded on dynein. RabB is the major player in establishing this "degradative identity," as it is required for EE movement and mediates recruitment of Vps45 and Vps34 to endosomes (not depicted; Abenza *et al.*, 2010). Vps45 enables endosomes to accept Golgi traffic required for maturation, whereas Vps34 synthesizes phosphatidyl inositol-3-phosphate, the landmark of degradative endosome identity, initiating the MVB pathway at the stage of EEs (Abenza *et al.*, 2010; Hervás-Aguilar *et al.*, 2010). RabB and, less efficiently, RabA recruit CORVET, mediating homotypic fusion between EEs, with key involvement of Vps8 (Markgraf *et al.*, 2009). As endosomes increase their size, they decrease their motility and acquire their final composition (*i.e.* become LEs). Then RabS^{Rab7} substitutes Rab5s. Finally, LEs undergo further fusion between them and with vacuoles in a HOPS-dependent manner. The negative feedback loop that may help to release Rab5s from endosomes is depicted.

0.1% fructose, or a combination of 1% ethanol and 0.02% glucose during 72 h at the indicated temperatures.

A. nidulans vps18 (*digA*), *Vac1*, *vps41*, and *gdiA* were identified as AN2266, AN3144, AN4876, and AN5895, respectively, in the *A. nidulans* genomic database. Deletion cassettes were constructed by PCR (Szewczyk *et al.*, 2006), using primers listed in Supplemental Table S3 and *Aspergillus fumigatus pyrG*^{Af} (for *vps18*Δ, *rabS*Δ, *vac1*Δ, and *vps41*Δ) or *pyroA*^{Af} (for a second *rabS*Δ deletion allele) as selection markers. Recipient strains carried *nkuA*Δ, preventing nonhomologous recombination (Nayak *et al.*, 2006). Constructs for integrative transformation were confirmed by sequencing. They were targeted to the *pyroA* or *argB* locus after transformation, using published methodology (Calcagno-Pizarelli *et al.*, 2007; Pantazopoulou and Peñalva, 2009). Single-copy integration was verified by Southern blots.

Western blotting

To determine levels of GFP-RabS^{Rab7} by Western blotting, we extracted proteins as described (Hervás-Aguilar *et al.*, 2007). GFP fusion proteins were detected using mouse anti α-GFP (monoclonal cocktail, 1:5000; Roche, Indianapolis, IN). Actin (detected with mouse anti α-actin from ICN Biomedicals (Irvine, CA) using 1:80,000 dilution of the antibody) was used as loading control. For the extraction of AgtA-GFP we used a reported procedure (Hervás-Aguilar and Peñalva, 2010) involving solubilization of proteins from lyophilized mycelial biomass with NaOH, followed by their precipitation with trichloroacetic acid.

Microscopy

Cells were grown in submerged cultures at 25°C in watch minimal medium (WMM), using Lab-Tek chambers (Nalge Nunc International, Rochester, NY) for 14–16 h before proceeding to microscopy (Pantazopoulou and Peñalva, 2009). To modulate the expression levels of the fluorescent chimeras expressed under the control of *alcA*^{p}, we used different carbon sources (Abenza *et al.*, 2009): low levels were attained with 0.1% (wt/vol) fructose, and high levels were obtained using 1% ethanol (vol/vol) or by preculturing cells on 0.02–0.05% (wt/vol) glucose and shifting them to 1% (vol/vol) ethanol for 3–4 h. In RabA-RabS^{Rab7} and in RabB-RabS^{Rab7} colocalization experiments, intermediate expression levels were achieved by culturing cells in WMM containing 1% (vol/vol) glycerol as carbon source. Mature endosomes/vacuoles were detected with CMAC as described (Abenza *et al.*, 2009; Pantazopoulou and Peñalva, 2009). To determine the effects of the *nudA1*^{ts} mutation, cells were cultivated at 37°C, which is a semirestrictive temperature, or overnight at 25°C (permissive temperature) and then shifted to 37°C for a few hours before image acquisition. To impede movement of *rabS*Δ minivacuoles, benomyl was added to WMM at a final concentration of 4.8 μg/ml as described (Abenza *et al.*, 2009). For experiments involving delivery of AgtA-GFP to the vacuole, cells were cultured at 25°C for 14–16 h in WMM containing 5 mM L-glutamate as nitrogen source and then shifted to the same medium in which 5 mM ammonium tartrate substituted for L-glutamate. AgtA-GFP images were taken at the 0-min time point and 80 min after the shift (Abenza *et al.*, 2009, 2010).

Images were acquired using a Hamamatsu ORCA ER-II camera (Hamamatsu, Hamamatsu, Japan) coupled to a Leica DMI6000B microscope (Leica, Wetzlar, Germany) driven by MetaMorph software (Molecular Dynamics, Sunnyvale, CA) and equipped with an EL6000 external light source for epifluorescence excitation. The microscope was equipped with HCX 63×, 1.4 numerical aperture (NA), and 100×, 1.4 NA, objectives and BrightLine GFP-3035B (Semrock, Rochester, NY), TXRED-4040B (mCherry), and standard

4′,6-diamidino-2-phenylindole (CMAC) filter sets. For colocalization experiments, a strictly simultaneous imaging of GFP and mCherry was carried out using a Dual-View imaging system (Photometrics, Tucson, AZ), using the recommended filter set (Pantazopoulou and Peñalva, 2011). MetaMorph software was used for contrast adjustment, Dual-View channel alignments, color combining, *z*-stack maximal-intensity projections (contrasted, when indicated, with the MetaMorph "unsharp mask" filter) and for the assembly of kymographs from time-lapse series. Images were converted to 8-bit grayscale (and usually shown in inverted contrast) or to 24-bit RGB and annotated with Corel Draw (Corel, Ottawa, Canada). For some *z*-stacks we improved image quality by using a blind deconvolution procedure (AutoDeblur software; Media Cybernetics, Bethesda, MD). Time-lapse sequences were converted to QuickTime using ImageJ 1.37 (National Institutes of Health, Bethesda, MD). Statistical analyses were performed using GraphPad Prism 5.00 for Windows (GraphPad Software, La Jolla, CA).

Affinity purification of RabS^{Rab7} effectors

Affinity purification of effectors using GDP- or GTP-γ-S GST-RabS^{Rab7} glutathione-Sepharose beads was made as described for GST-RabB. Glutathione-Sepharose 4B beads containing GST-RabS^{Rab7} were incubated with *A. nidulans* protein extracts in 50-ml Falcon tubes before eluting the interacting proteins, which were resolved by SDS–PAGE cells, excised, and analyzed by matrix-assisted laser desorption/ionization peptide mass fingerprinting and tandem mass spectrometry (MS/MS), as detailed (Abenza *et al.*, 2010).

ACKNOWLEDGMENTS

We thank E. Reoyo for technical assistance. This work was supported by the Spanish government through Dirección General de Investigación Científica y Técnica Grant BIO2009-7281 and by Comunidad de Madrid Networking Grant SAL/0246/2006 to M.A.P. J.F.A. was a Consejo Superior de Investigaciones Cientificas I3P predoctoral fellow.

REFERENCES

Abenza JF, Galindo A, Pantazopoulou A, Gil C, de los Ríos V, Peñalva MA (2010). *Aspergillus* RabB^{Rab5} integrates acquisition of degradative identity with the long-distance movement of early endosomes. Mol Biol Cell 21, 2756–2769.

Abenza JF, Pantazopoulou A, Rodríguez JM, Galindo A, Peñalva MA (2009). Long-distance movement of *Aspergillus nidulans* early endosomes on microtubule tracks. Traffic 10, 57–75.

Angers CG, Merz AJ (2009). HOPS interacts with Apl5 at the vacuole membrane and is required for consumption of AP-3 transport vesicles. Mol Biol Cell 20, 4563–4574.

Apostolaki A, Erpapazoglou Z, Harispe L, Billini M, Kafasla P, Kizis D, Peñalva MA, Scazzocchio C, Sophianopoulou V (2009). AgtA, the dicarboxylic amino acid transporter of *Aspergillus nidulans*, is concertedly down-regulated by exquisite sensitivity to nitrogen metabolite repression and ammonium-elicited endocytosis. Eukaryot Cell 8, 339–352.

Araujo-Bazán L, Peñalva MA, Espeso EA (2008). Preferential localization of the endocytic internalization machinery to hyphal tips underlies polarization of the actin cytoskeleton in *Aspergillus nidulans*. Mol Microbiol 67, 891–905.

Balderhaar HJ, Arlt H, Ostrowicz C, Brocker C, Sundermann F, Brandt R, Babst M, Ungermann C (2010). The Rab GTPase Ypt7 is linked to retromer-mediated receptor recycling and fusion at the yeast late endosome. J Cell Sci 123, 4085–4094.

Behnia R, Munro S (2005). Organelle identity and the signposts for membrane traffic. Nature 438, 597–604.

Brocker C, Engelbrecht-Vandre S, Ungermann C (2010). Multisubunit tethering complexes and their role in membrane fusion. Curr Biol 20, R943–R952.

Cabrera M *et al.* (2010). Phosphorylation of a membrane curvature-sensing motif switches function of the HOPS subunit Vps41 in membrane tethering. J Cell Biol 191, 845–859.

Calcagno-Pizarelli AM, Hervás-Aguilar A, Galindo A, Abenza JF, Peñalva MA, Arst HN Jr (2011). Rescue of *Aspergillus nidulans* severely debilitating null mutations in ESCRT-0, I, II and III genes by inactivation of a salt-tolerance pathway allows examination of ESCRT gene roles in pH signalling. J Cell Sci 124, 1–13.

Calcagno-Pizarelli AM *et al.* (2007). Establishment of the ambient pH signaling complex in *Aspergillus nidulans*: PalI assists plasma membrane localization of PalH. Eukaryot Cell 6, 2365–2375.

Cove DJ (1966). The induction and repression of nitrate reductase in the fungus *Aspergillus nidulans*. Biochim Biophys Acta 113, 51–56.

Findon H, Calcagno-Pizarelli AM, Martínez JL, Spielvogel A, Markina-Iñarrairaegui A, Indrakumar T, Ramos J, Peñalva MA, Espeso EA, Arst HN Jr (2010). Analysis of a novel calcium auxotrophy in *Aspergillus nidulans*.. Fungal Genet Biol 47, 647–655.

Galindo A, Calcagno-Pizarelli AM, Arst HN Jr, Peñalva MA (2012). An ordered pathway for the assembly of ESCRT-containing fungal ambient pH signalling complexes at the plasma membrane. J Cell Sci 125, 1784–1795.

Galindo A, Hervás-Aguilar A, Rodríguez-Galán O, Vincent O, Arst HN Jr, Tilburn J, Peñalva MA (2007). PalC, one of two Bro1 domain proteins in the fungal pH signaling pathway, localizes to cortical structures and binds Vps32. Traffic 8, 1346–1364.

Geissenhoner A, Sievers N, Brock M, Fischer R (2001). *Aspergillus nidulans* DigA, a potential homolog of *Saccharomyces cerevisiae* Pep3 (Vps18), is required for nuclear migration, mitochondrial morphology and polarized growth. Mol Genet Genomics 266, 672–685.

Griffith J, Peñalva MA, Reggiori F (2011). Adaptation of the Tokuyasu method for the ultrastructural study and immunogold labelling of filamentous fungi. J Electron Microsc 60, 211–216.

Hervás-Aguilar A, Peñalva MA (2010). Endocytic machinery protein SlaB is dispensable for polarity establishment but necessary for polarity maintenance in hyphal tip cells of *Aspergillus nidulans*. Eukaryot Cell 9, 1504–1518.

Hervás-Aguilar A, Rodríguez JM, Tilburn J, Arst HN Jr, Peñalva MA (2007). Evidence for the direct involvement of the proteasome in the proteolytic processing of the *Aspergillus nidulans* zinc finger transcription factor PacC. J Biol Chem 282, 34735–34747.

Hervás-Aguilar A, Rodríguez-Galán O, Galindo A, Abenza JF, Arst HN Jr, Peñalva MA (2010). Characterization of *Aspergillus nidulans* DidB^{Did2}, a non-essential component of the multivesicular body pathway. Fungal Genet Biol 47, 636–646.

Huotari J, Helenius A (2011). Endosome maturation. EMBO J 30, 3481–3500.

Jordens I, Fernández-Borja M, Marsman M, Dusseljee S, Janssen L, Calafat J, Janssen H, Wubbolts R, Neefjes J (2001). The Rab7 effector protein RILP controls lysosomal transport by inducing the recruitment of dynein-dynactin motors. Curr Biol 11, 1680–1685.

Kinchen JM, Ravichandran KS (2010). Identification of two evolutionarily conserved genes regulating processing of engulfed apoptotic cells. Nature 464, 778–782.

Lenz JH, Schuchardt I, Straube A, Steinberg G (2006). A dynein loading zone for retrograde endosome motility at microtubule plus-ends. EMBO J 25, 2275–2286.

Markgraf DF, Ahnert F, Arlt H, Mari M, Peplowska K, Epp N, Griffith J, Reggiori F, Ungermann C (2009). The CORVET subunit Vps8 cooperates with the Rab5 homolog Vps21 to induce clustering of late endosomal compartments. Mol Biol Cell 20, 5276–5289.

Nayak T, Szewczyk E, Oakley CE, Osmani A, Ukil L, Murray SL, Hynes MJ, Osmani SA, Oakley BR (2006). A versatile and efficient gene targeting system for *Aspergillus nidulans*. Genetics 172, 1557–1566.

Nordmann M, Cabrera M, Perz A, Brocker C, Ostrowicz C, Engelbrecht-Vandre S, Ungermann C (2010). The Mon1-Ccz1 complex is the GEF of the late endosomal Rab7 homolog Ypt7. Curr Biol 20, 1654–1659.

Ohsumi K, Arioka M, Nakajima H, Kitamoto K (2002). Cloning and characterization of a gene (avaA) from *Aspergillus nidulans* encoding a small GTPase involved in vacuolar biogenesis. Gene 291, 77–84.

Oka M, Maruyama J, Arioka M, Nakajima H, Kitamoto K (2004). Molecular cloning and functional characterization of avaB, a gene encoding Vam6p/Vps39p-like protein in *Aspergillus nidulans*. FEMS Microbiol Lett 232, 113–121.

Ostrowicz CW, Brocker C, Ahnert F, Nordmann M, Lachmann J, Peplowska K, Perz A, Auffarth K, Engelbrecht-Vandre S, Ungermann C (2010). Defined subunit arrangement and Rab interactions are required for functionality of the HOPS tethering complex. Traffic 11, 1334–1346.

Pantazopoulou A, Peñalva MA (2009). Organization and dynamics of the *Aspergillus nidulans* Golgi during apical extension and mitosis. Mol Biol Cell 20, 4335–4347.
Pantazopoulou A, Peñalva MA (2011). Characterization of *Aspergillus nidulans* RabC^{Rab6}. Traffic 12, 386–406.
Peñalva MA (2005). Tracing the endocytic pathway of *Aspergillus nidulans* with FM4-64. Fungal Genet Biol 42, 963–975.
Peñalva MA (2010). Endocytosis in filamentous fungi: Cinderella gets her reward. Curr Opin Microbiol 13, 684–689.
Peplowska K, Markgraf DF, Ostrowicz CW, Bange G, Ungermann C (2007). The CORVET tethering complex interacts with the yeast Rab5 homolog Vps21 and is involved in endo-lysosomal biogenesis. Dev Cell 12, 739–750.
Pfeffer S, Aivazian D (2004). Targeting Rab GTPases to distinct membrane compartments. Nat Rev Mol Cell Biol 5, 886–896.
Poteryaev D, Datta S, Ackema K, Zerial M, Spang A (2010). Identification of the switch in early-to-late endosome transition. Cell 141, 497–508.
Price A, Seals D, Wickner W, Ungermann C (2000). The docking stage of yeast vacuole fusion requires the transfer of proteins from a cis-SNARE complex to a Rab/Ypt protein. J Cell Biol 148, 1231–1238.
Rieder SE, Emr SD (1997). A novel RING finger protein complex essential for a late step in protein transport to the yeast vacuole. Mol Biol Cell 8, 2307–2327.
Rink J, Ghigo E, Kalaidzidis Y, Zerial M (2005). Rab conversion as a mechanism of progression from early to late endosomes. Cell 122, 735–749.
Rodríguez-Galán O, Galindo A, Hervás-Aguilar A, Arst HN Jr, Peñalva MA (2009). Physiological involvement in pH signalling of Vps24-mediated recruitment of Aspergillus PalB cysteine protease to ESCRT-III. J Biol Chem 284, 4404–4412.
Sánchez-Ferrero JC, Peñalva MA (2006). Endocytosis. In: The Aspergilli: Genomics, Medical Aspects, Biotechnology, and Research Methods, eds. GH Goldman, SA Osmani, Boca Raton, FL: CRC Press, 177–195.
Schuster M, Lipowsky R, Assmann MA, Lenz P, Steinberg G (2011). Transient binding of dynein controls bidirectional long-range motility of early endosomes. Proc Natl Acad Sci USA 108, 3618–3623.
Seals DF, Eitzen G, Margolis N, Wickner WT, Price A (2000). A Ypt/Rab effector complex containing the Sec1 homolog Vps33p is required for homotypic vacuole fusion. Proc Natl Acad Sci USA 97, 9402–9407.
Segev N (2011). Coordination of intracellular transport steps by GTPases. Semin Cell Dev Biol 22, 33–38.
Steinberg G (2007). On the move: endosomes in fungal growth and pathogenicity. Nat Rev Microbiol 5, 309–316.
Szewczyk E, Nayak T, Oakley CE, Edgerton H, Xiong Y, Taheri-Talesh N, Osmani SA, Oakley BR (2006). Fusion PCR and gene targeting in *Aspergillus nidulans*.. Nat Protoc 1, 3111–3120.
Taheri-Talesh N, Horio T, Araujo-Bazán L, Doux X, Espeso EA, Peñalva MA, Osmani SA, Oakley BR (2008). The tip growth apparatus of *Aspergillus nidulans*. Mol Biol Cell 19, 1439–1449.
Wedlich-Soldner R, Straube A, Friedrich MW, Steinberg G (2002). A balance of KIF1A-like kinesin and dynein organizes early endosomes in the fungus *Ustilago maydis*. EMBO J 21, 2946–2957.
Zekert N, Fischer R (2008). The *Aspergillus nidulans* kinesin-3 UncA motor moves vesicles along a subpopulation of microtubules. Mol Biol Cell 20, 673–684.
Zerial M, McBride H (2001). Rab proteins as membrane organizers. Nat Rev Mol Cell Biol 2, 107–117.
Zhang J, Yao X, Fischer L, Abenza JF, Penalva MA, Xiang X (2011). The p25 subunit of the dynactin complex is required for dynein-early endosome interaction. J Cell Biol 193, 1245–1255.
Zhang J, Zhuang L, Lee Y, Abenza JF, Peñalva MA, Xiang X (2010). The microtubule plus-end localization of *Aspergillus* dynein is important for dynein-early-endosome interaction but not for dynein ATPase activation. J Cell Sci 123, 3596–3604.